Solvent-free Preparation of Ru/Al 2 O 3 Catalysts for CO 2 Methanation: An Example of Frugal Innovation

Ryma Haddad, Yingrui Zhao, Antoine Miche, Ferdaous Ben Romdhane, Nivedita Sudheer, Ovidiu Ersen, François Devred, François Ribot, Capucine Sassoye, Clement Sanchez, et al.

Solvent-free Preparation of Ru/Al_2O_3 Catalysts for CO_2 Methanation: An Example of Frugal Innovation

Published as part of the Chemistry of Materials virtual special issue "In Honor of Prof. Clement Sanchez".

Ryma Haddad, Yingrui Zhao, Antoine Miche, Ferdaous Ben Romdhane, Nivedita Sudheer, Ovidiu Ersen, François Devred, François Ribot, Capucine Sassoye, Clement Sanchez, Damien P. Debecker, Corinne Chaneac,* and Cédric Boissière*

ABSTRACT: To reduce the environmental impact of supported catalyst production in compliance with the recommendations of the UN's 12th objective, which encourages more sustainable consumption and production patterns, we propose to revisit sol–gel chemistry in a more frugal mode. The principle of frugal innovation is to simplify products and processes, eliminate complexities to make solutions easier to understand and use, and reduce production costs. By this way, the synthesis of ruthenium-based catalysts supported on γ-AlOOH and γ-Al_2O_3 is revised via solvent-free sol–gel chemistry. Such catalysts are successfully prepared in one-pot preparation of the active phase and the support using $Ru(acac)_3$/Al alkoxide that requires no sacrificial organic pore-generating agent, no washing, and no filtration and produces no liquid waste. The mixed Ru/Al precursor is hydrolyzed with a stoichiometric amount of water without any solvent. The obtained materials containing 1 and 3% Ru/Al molar ratios have high specific surface areas, from 300 to 690 $m^2 \cdot g^{-1}$ and exhibit well dispersed NPs of 1–4 nm on γ-AlOOH with interesting CO_2 methanation activity and 100% CH_4 selectivity. This proves that a frugal synthesis approach can do as well as traditional synthesis methods while having a much lower environmental impact (cE-factor, water consumption, and energy consumption are 24, 69, and 24 to 42 times lower, respectively) than the standard multistep protocol..

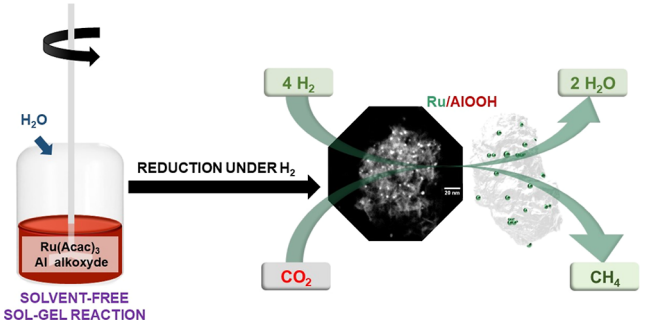

1. INTRODUCTION

Industries play a crucial role in achieving sustainable development goals and must evolve to reduce their impact on the planet while ensuring its prosperity.[1,2] Catalysis is a lever for solving global socio-economic challenges such as the continuous growth in energy and natural depletable resource requirements in numerous application fields including health (drug or protein synthesis),[3,4] energy (oil refining and small molecule valorization),[5−8] bioresources transformation, and environmental remediation.[9−11] Therefore, there is a research craze for the development of new supported heterogeneous catalysts.[12]

The synthesis of such catalysts typically involves several main physical or chemical routes. The latter, such as impregnation or deposition–precipitation of the support material with a solution containing the desired catalyst precursor,[8,13−18] as well as aerosol processing of heterogeneous catalysts, are common at the industrial scale.[19] Most of the time, these methods require a high volume of solvent and additives, use several devices and heating treatments, and thus consume a lot of energy and atoms. Therefore, it became important to take into account the environmental friendliness, energy, and atom economy, as well as the ease of industrial processability of the heterogeneous catalyst materials production.

One of the promising synthetic approaches for limiting the production of waste and consume less energy is to develop solvent-less synthesis strategies. Recent studies[20−28] mention the facile synthesis of various metal oxides and mixed oxides for catalytic activity (Al_2O_3[23] and Cu,[29] La,[30] Pd[25] or MnO_x-doped Al_2O_3,[31] Ni oxide and hydroxide,[32,33] CuO,[34] Fe_2O_3,[26] Ni and ZrO_2 doped CeO_2, or Ni doped ZnO and iron phosphide catalysts) by solvent-less mechanosynthesis methods using ammonium bicarbonate (NH_4HCO_3) and hydrated metal nitrates or metal chloride in stoichiometric proportions.

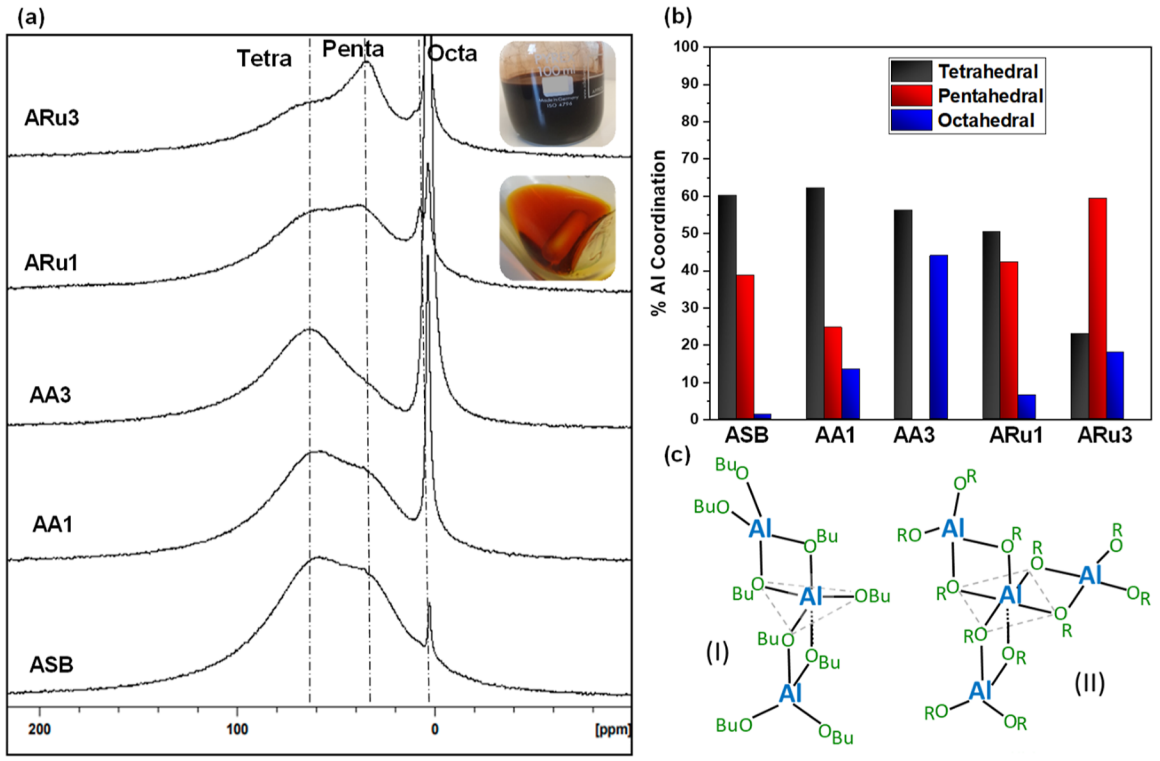

Figure 1. (a) ^{27}Al NMR spectra in $CDCl_3$ of reactants: ASB, reactive media ASB + $Ru(acac)_3$ with Ru/Al 1 and 3%, and mixed ASB with AcacH (with the same AcacH concentrations equivalent to those of 1 and 3% $Ru(acac)_3$ mixtures); (b) proportion of different Al coordinations determined from the deconvolution of ^{27}Al NMR spectra (Figures S1–S5); (c) structure models of ASB species according to literature, with I being the major species.[37−40]

This approach requires several washing steps (for removing large quantities of ammonium salt byproducts) and/or a calcination step producing HNO_3 (or HCl) and ammonia. This processing reduces drastically the final crystallite size if compared with a standard precipitation method, which may be an advantage for producing high-surface-area materials.[26,35] In another approach, Huang et al. reported a solvent-deficient synthesis of mesoporous gamma alumina starting from the reaction of aluminum alkoxides and very small quantities of water using hand mortar.[23] While the chemical approach is interesting in this example, industrial-scale production is very difficult to set up and requires other tools for shaping the catalyst.

In a recent study,[36] we used a continuous reactive extrusion process for the solvent-free production of high-surface-area mesoporous γ-AlOOH and γ-Al_2O_3 extrudates. The easy scale-up, global low atom and energy consumption, and drastic reduction of the quantity of chemical waste make this synthesis strategy a very realistic method for improving the actual nanoporous alumina catalysts production. Yet, so far, only pure alumina support is produced by this method, and nothing is reported on the extension of such solvent-free synthesis for the integrative preparation of supported heterogeneous catalysts.

In this manuscript, we extend our solvent-free approach for the preparation of heterogeneous catalysts combining γ-AlOOH support and ultrasmall ruthenium nanoparticles (Ru NPs) of 1−4 nm as the metallic active phase. To achieve this, a very simple, affordable, and minimalist batch process based on solvent-free sol−gel chemistry is used for the preparation of a mixed Ru−Al alkoxide precursor. We investigated the impact of the mixed sol−gel precursor on the boehmite formation as well as the dispersion of ruthenium in the support and its ability to be reduced and to form nanoclusters or nanoparticles in this peculiar solvent-free strategy. Ru-based catalytic materials activities toward the thermal hydrogenation of CO_2 to methane are measured and compared to similar Ru/Al_2O_3 catalysts prepared by the incipient wetness impregnation method, where the γ-Al_2O_3 was prepared by the same solvent-free sol−gel method.[22] Herein, we also present an attempt to compare the solvent-free sol−gel production of a Ru/ supported catalyst with the classical impregnation approach.

2. RESULTS AND DISCUSSION

2.1. Reactive Medium Characterizations. Catalysts of boehmite (AlOOH) doped with ruthenium (Ru) were obtained by first preparing a reactive sol−gel precursor consisting of the dissolution of $Ru(acac)_3$ solid in pure aluminum trisec-butoxide (ASB, viscous liquid). Samples were made with Ru/Al molar ratios of 1%, named ARu1, and 3%, named ARu3 (corresponding to Ru/AlOOH 1.69 and 5.08 wt % or corresponding to Ru/Al_2O_3 2 and 6 wt %), without adding any solvent or other chemicals. After aging at 130 °C for 8 h in oven, the mixture consists in homogeneous orange solution for ARu1 and a dark brown saturated solution for ARu3. Each Ru/Al mixture remains stable for several months after synthesis.

In order to understand the reaction that occurs between $Ru(acac)_3$ and ASB, the two Ru-ASB mixtures are studied by liquid ^{27}Al NMR spectroscopy and compared with two references containing ASB and acetylacetone (AcacH) of the same molar ratio. Each as-prepared mixture is diluted in $CDCl_3$ (6−8 wt %) before analysis.

The spectrum of ASB (Figure 1) presents a broad asymmetric signal with a maximum at 61 ppm related to

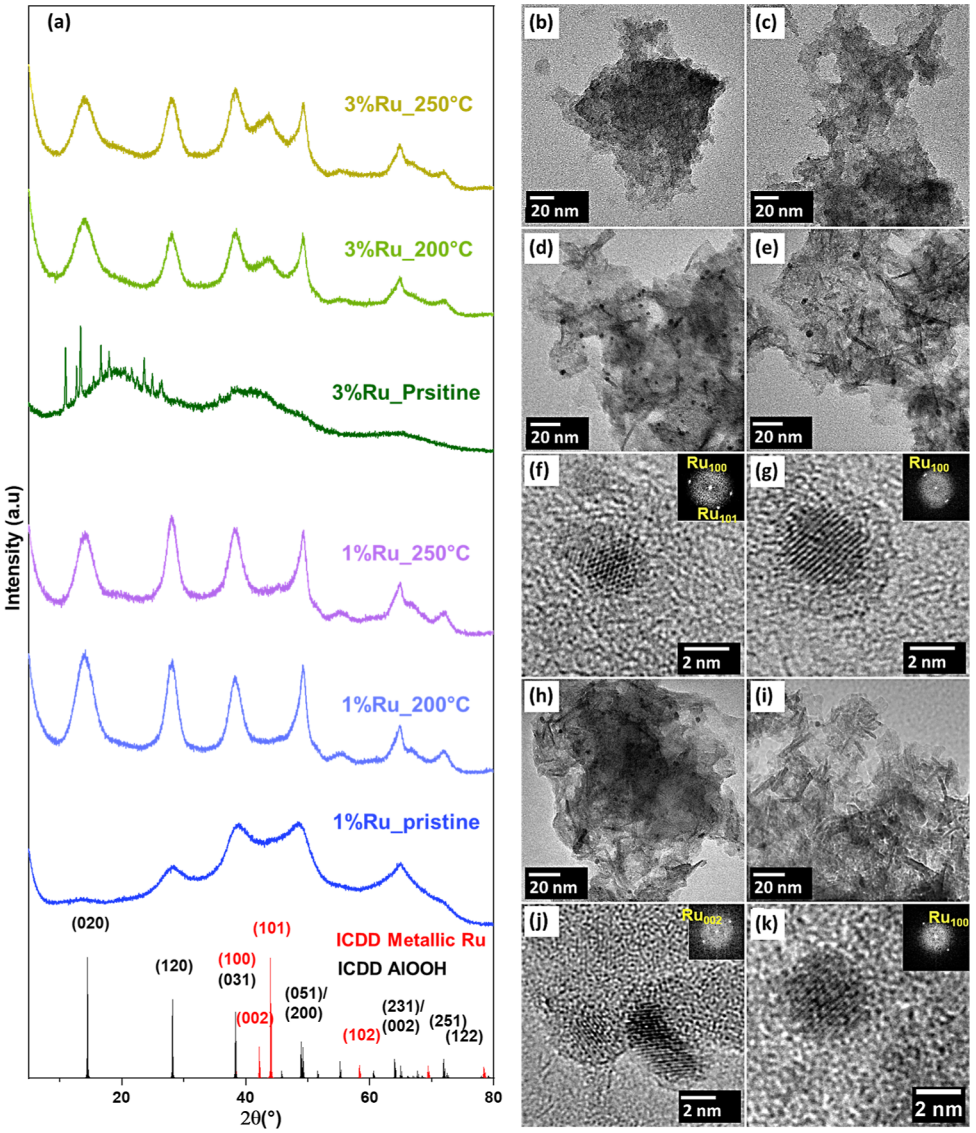

Figure 2. (a) Powder X-ray diffraction patterns of references, AlOOH ICDD 00-021-1307, metallic Ru ICDD 01-070-0274, and of Ru1% and Ru3% samples, before (pristine) and after reduction under pure H2 at 200 and 250 °C. TEM image of (b) 1%Ru_pristine and (c) 3%Ru_pristine samples before reduction. TEM image of powders reduced at 200 °C under H2: (d) 1%Ru_200 °C and (e) 3%Ru_200 °C; corresponding HR-STEM (f) 1%Ru_200 °C and (g) 3%Ru_200 °C. TEM image of powders reduced at 250 °C under H2: (h)1%Ru_250 °C and (i) 3%Ru_250 °C; corresponding HR-STEM (j) 1%Ru_250 and (k) 3%Ru_250. The insets of pictures f, g, j, and k are FFT of the nanocrystals.

tetra-coordinated sites, a shoulder around 31 ppm for the penta-coordinated sites, as well as a small sharp peak at 2.7 ppm that is assigned to hexa-coordinated aluminum centers.[37−41] With the addition of AcacH, the ^{27}Al NMR spectra of AA1 and AA3 show different features from the spectra of ASB. A reorganization of the aluminum coordination can be noticed with a progressive decrease of the peak at 31 ppm associated with the penta-coordinated centers and the growth of the Al hexa-coordinated centers when wt % AcacH increases. This indicates that AcacH reacts with ASB in a preferential attack on the central penta-coordinated Al atoms (the species I in Figure 1c), leading to the formation of six-coordinated structural units. This result is in agreement with previous reported studies.[38−41] Modifications are confirmed by the appearance of signals at 1.99 and 5.57 ppm in the ^{1}H NMR spectra (Figure S6), which correspond respectively to the methyl ($-CH_3$) and methine ($-CH$) protons of the acetylacetonate (Acac) ligand linked to an Al atom. Compared to ASB, the proportion of tetra-coordinated sites decreases slightly on ARu1, and those of penta-coordinated sites and those of hexa-coordinated sites increase slightly. The observation of two resonances around 7 ppm seems to indicate the existence of two different octahedral aluminum centers for ARu1 (Figure S4). Moreover, on the ^{1}H NMR spectrum (Figure S6), the absence of signals at −5.57 and −30.29 ppm, which correspond respectively to the methyl and methine protons of $Ru(acac)_3$,[42,43] indicates that the ruthenium center has lost its acetylacetonate (Acac) ligands. The appearance of two peaks at 5.57 and 1.99 ppm, corresponding to the Acac coordinated on Al,[44] shows that the acetylacetonate ligands have moved onto aluminum atoms, which are likely the peripheral ones according to the evolution of the aluminum coordination observed by ^{27}Al NMR. The observation of a new signal around −22 ppm in the ^{1}H NMR spectrum of ARu1 tends to indicate that the Acac ligands are replaced by new hydrogenated species (*sec*-BuO, OH, etc.). ARu3 significantly decreases the tetracoordinate sites, and

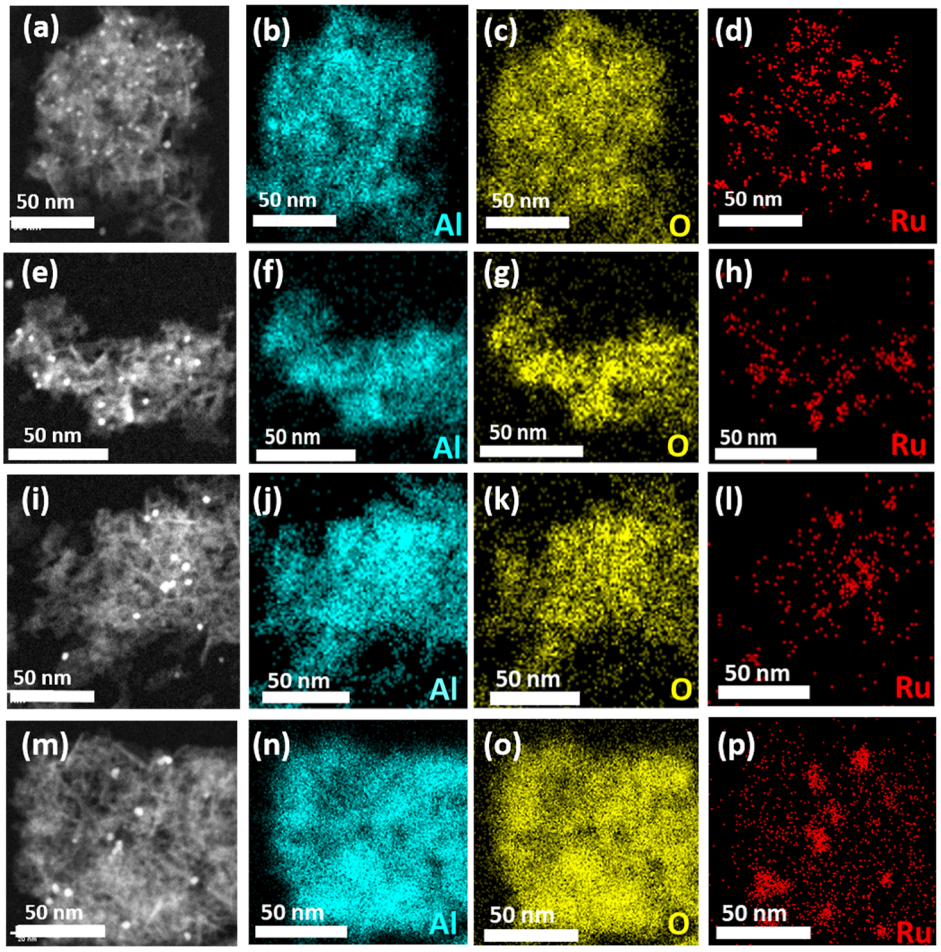

Figure 3. HAADF-STEM images of the reduced samples: (a) 1%Ru_200 °C and it is corresponding EDX elemental maps (b–d) measured on Al (blue), O (yellow), and Ru (red). (e) HAADF-STEM image of 1%Ru_250 °C and its corresponding EDX elemental maps (f)–h). (i) HAADF-STEM image of 3%Ru_200 °C and its corresponding EDX elemental maps (j–l). (m) HAADF-STEM images of 3%Ru_250 °C and its corresponding EDX elemental maps (n–p).

there is an increase in pentacoordinate and octahedral sites, which may indicate an attack on the peripheral tetracoordinated Al atoms. Even though we could not find evidence of the formation of a mixed Ru–Al alkoxide, a ligand exchange and a Ru-induced effect occur, leading to good homogeneity of the two metallic species.

2.2. Structural Characterizations of Ru-Based Catalysts (Powders). The previous liquid mixtures were hydrolyzed (with a hydrolysis ratio of h = H_2O/Al = 5) using a mechanical anchor in a batch reactor. This very simple procedure leads to the formation of gels that are transformed into powders after drying. The remaining traces of alcohol produced by the hydrolysis reaction are removed under vacuum at 25 °C. They were labeled Ru1%_Pristine and Ru3%_Pristine.

The Ru/Al molar ratios determined by X-ray fluorescence spectroscopy (XRF) were 0.8% and 3.1% for Ru1%_Pristine and Ru3%_Pristine samples, respectively. The global composition is in good agreement with the expected one, considering the experimental parameters.

X-ray diffraction analysis (XRD) (Figure 2a) of Ru1%_Pristine exhibits very broad diffraction peaks characteristic of a poorly structured boehmite. After heating under H_2 at 200 and 250 °C, peaks are sharper, indicating an increase of boehmite crystallinity. However, no additional peak of crystalline ruthenium species is detected in XRD, probably due to the very small Ru content or the very small size of the Ru domains. The diffraction diagram of 3%Ru_Pristine is characteristic of amorphous aluminum oxi-hydroxide material superimposed on sharp peaks below 30° corresponding to $Ru(acac)_3$ crystals. After heating under H_2, $Ru(acac)_3$ crystalline peaks disappear and AlOOH peaks are clearly identified, indicating a better structuration of the aluminum oxi-hydroxide network. In addition, we observe the appearance of a broad peak at $2\theta = 44°$, indicative of the (101) peak of hc-Ru.

Transmission electron microscopy (TEM) of the 1% Ru_Pristine sample (Figure 2. (b)) exhibits no high electronic density aggregate, while very few particles of about 2 nm are visible in 3%Ru_Pristine powder. After hot reduction, well-dispersed particles of 2.5 nm on average are clearly identified on the high-resolution transmission electron microscopy (HRTEM) image. A counting of particle size distributions given in Supporting Information 11 evidence that very little difference exists (2.7 vs 2.3 nm on average, with an error bar of 0.5 nm) after reduction at 200 and 250 °C respectively. The fast Fourier transform (FFT) of the high-resolution scanning transmission electron microscopy (STEM) confirms that it is indeed metallic ruthenium nanoparticles. In parallel, TEM and STEM images at high resolution indicate nanoparticles of 3.7

nm on average well dispersed on the boehmite sheets. A counting of particle size distributions given in Supporting Information 11 evidence that very little difference exists (3.5 vs 3.8 nm in average, with an error bar or 0.5 nm) after reduction at 200 and 250 °C.

The FFT of the STEM at high resolution confirms that it is indeed metallic ruthenium.

The HAADF-STEM images confirm the good dispersion of Ru particles all over the AlOOH support (Figure 3). The STEM tomography was carried out on the sample 3%Ru_250 °C (Video S1). The dark field data processing allowed us to observe the distribution of Ru nanoparticles on the surface of the mesoporous network of the boehmite support.

Textural analysis by N_2 physisorption of the aluminum-based reference 0%Ru_pristine shows that the solvent-free synthesis produced a high surface area and high-volume material with 725 and 1.72 $cm^3 \cdot g^{-1}$, respectively (Supporting Information 12). All samples exhibit isotherms that belong to type IV, with a characteristic hysteresis loop associated with slit-shaped opened mesopores (Figure S7). Brunauer–Emmett–Teller (BET) surface areas (Table 1) of the reference and ruthenium-loaded samples are very high, ranging from 300 to 725 $m^2 \cdot g^{-1}$. These values are comparable to the highest values reported for mesoporous alumina prepared from aluminum alkoxide in optimized Yoldas synthesis using chelating agents (optimal acacH/ASB mole ratios),[45] peptization, and pretreatment under vacuum of the obtained gels after synthesis.[46] The pore volumes of the materials range from 0.63 to 1.72 $cm^3 \cdot g^{-1}$ (Table 1). They are comparable to pore volumes of ordered mesoporous alumina prepared via surfactant-induced fiber formation.[47] These large pore volumes can be attributed to intercrystalline cavities created by randomly stacked AlOOH nanosheets.[23] We observed that, for nontreated pristine materials, the introduction of 1 wt % and 3% of ruthenium centers induces a progressive loss of surface area and porous volume. This decrease of textural properties is coherent with the progressive loss of structural order observed by XRD, indicating smaller crystalline domains, which are likely to form more compact structures. One has to notice, however, that the incorporation of ruthenium centers also induces the introduction of acetylacetonate ligands that are still trapped within the structure and contribute to the decrease in surface area and porous volume, maybe by blocking some porosity.

Table 1. BET Surfaces and Pore Volumes of the Sample According to N_2 Physisorption

sample	BET surface area ($m^2 \cdot g^{-1}$)	pore volume ($cm^3 \cdot g^{-1}$)
0%Ru_pristine	725	1.72
1%Ru_pristine	688	1.16
1%Ru_200 °C	337	1.08
1%Ru_250 °C	435	1.51
3%Ru_pristine	507	0.65
3%Ru_200 °C	378	0.72
3%Ru_250 °C	302	0.63

The variations of textures observed after heat treatment at 200 °C (strong loss of surface area, while porous volume is little affected) are probably due to the progressive disappearance of acetylacetonate ligands and remaining alkoxide groups as well as to the recrystallization of the boehmite lattice observed in XRD. The decrease in surface area observed during heat treatment is consistent with the crystallization of the boehmite lattice (the improved stacking of AlOOH sheets during reduction results in the decrease of adsorption surface area). At this stage of the study, we cannot separate the contribution of heating (which allows desorption of organic residues and improved structural mobility) from the effect of ruthenium reduction (which perhaps leads also to the release of Al surface sites, favoring better crystallization of the boehmite network). Finally, textural evolutions observed after 250 °C reduction treatment probably result from progressive structural rearrangement (densification, pore opening, Ruthenium reduction, migration, etc.) that is not well understood yet. From these data, it is difficult to determine if Ru(0) particles are trapped within the boehmite deposited at its surface.

X-ray photoelectron spectrometry technique was employed additionally to establish the oxidation states of the surface ruthenium atoms before catalytic activity measurements. Figure S8 displays the XPS survey spectra for C 1s and Ru 3d of the six samples. The atomic percentages of Al and the different oxidation states of Ru are reported in Table S1. Both 1%Ru_pristine and 3%Ru_pristine indicate the presence of oxidized ruthenium (labeled RuO_x in this manuscript). After reduction under H_2 XPS, data show that all ruthenium centers in materials analyzed are not reduced. All samples indicate the presence of metallic Ru(0) with the ratio of Ru(0) to total Ru detected by XPS ($Ru_{(0)}/Ru_{tot}$) ranging between 39% (for 1% Ru_250) and 71% (for 3%Ru_250). Although we took as much precaution as possible to protect samples for XPS analyses, we know that air exposure is likely to promote surface reoxidation and thus decrease the $Ru(0)/Ru_{total}$ ratio. Yet, the large difference observed between samples is very likely the signature of the presence of nonreduced ruthenium centers after reduction at 200 and 250 °C.

Based on the data acquired so far, it is difficult to determine without ambiguity the exact localization of Ru centers after sol–gel polycondensation of the inorganic network, i.e., trapped within the alumina matrix or on the surface. Yet, considering that (i) the presence of ruthenium strongly affects the structuration of pristine materials, (ii) the coordinance of aluminum centers is affected by the presence of $Ru(acac)_3$, and (iii) all ruthenium centers are not fully reduced by H_2 treatment, we can assume that a part of the Ru centers is trapped within the boehmite network rather than deposited onto their surface and/or on boehmite nanocrystal edges.

From a catalytic point of view, the proportion of Ru(0) atoms effectively accessible on the surface of the catalyst (i.e., Ru dispersion, calculated as $Ru(0)_{surface}/Ru_{total}$) is a crucial parameter because it determines the amount of potentially active sites. The dispersion value was measured by H_2 chemisorption, assuming a chemisorption stoichiometry of H/Ru = 1 [8,48–50] (Table 2). The metal dispersion is calculated by dividing this value by the total amount of Ru present in the catalyst [Ru_{total}, measured by energy dispersive X-ray fluorescence (EDXRF)].

The catalyst reduced at 200 °C with 1% Ru loading displays a dispersion of 12%. The dispersion increases to 19% for the catalyst reduced at 250 °C. This result can potentially indicate that the heat treatment at 250 °C favors the migration of Ru species from the support matrix toward the surface, a phenomenon referred to as "exsolution", where they are more prone to reduction.[51] The catalysts with 3% Ru loading display Ru dispersion of 3.3 and 2.9% for 3%Ru_200 °C and

Table 2. Ruthenium Dispersion Determined by H_2 Chemisorption Analysis for the Samples Reduced at 200 and 250 °C

sample	H_2 adsorbed (μmol·g_{cat}^{-1})	dispersion (%)
1%Ru_200 °C	7.7	12.0
1%Ru_250 °C	11.8	19.0
3%Ru_200 °C	8.5	3.3
3%Ru_250 °C	7.4	2.9

3%Ru_250 °C, respectively, meaning that only a small quantity of metallic Ru is accessible for H_2 chemisorption.

2.3. Catalytic Activity Measurement toward CO_2 Methanation. These materials have structural and chemical properties that are very interesting for the thermocatalytic hydrogenation of CO_2 to CH_4. The catalytic performances toward CO_2 conversion and CH_4 production were measured for these reduced Ru/AlOOH materials prepared by direct solvent-free synthesis. The catalytic tests were carried out at 200, 250, and 300 °C at atmospheric pressure with a gas flow space velocity of 12,000 mL·g^{-1} h^{-1} and a H_2:CO_2 ratio of 4:1. Samples were activated in situ under H_2 at 200 °C.

When the reaction temperature increases from 200 to 300 °C, the CO_2 conversion logically increases for all of the catalysts (Figure 4a). As expected for Ru-based catalysts in this temperature range, the selectivity for CH_4 is 100%. Catalysts with a low loading of 1% Ru exhibit low CO_2 conversions (about 2%) at 200 °C and reach a maximum CO_2 conversion of 43% at 300 °C. The specific activity of these two samples, 1%Ru_200 °C and 1%Ru %_250 °C, is comparable at all the temperatures tested, reaching about 22 and 24 mmol·g_{cat}^{-1}·h^{-1} at 300 °C. The catalysts with higher loading, 3%Ru_200 °C and 3%Ru_250 °C, have CO_2 conversions of 11 and 12% at 200 °C and reach 66 and 54% at 300 °C, respectively. These conversions are comparable to those reported for catalysts in the literature.[52] The specific activity of the CH_4 production rate at 200 °C (at low conversion to remain in the differential conversion regime) (Figure 4b) are similar for 3%Ru_200 °C and 3%Ru_250 °C (6.1 and 6.2 mmol·g_{cat}^{-1}·h^{-1}, respectively). At 250 and 300 °C, the CH_4 production rate of 3%Ru_200 °C presents slightly higher activity than 3%Ru_250 °C.

Taking Ru dispersion into account, an "apparent TOF" can be calculated, here defined as the specific productivity normalized by the amount of $Ru_{surface}$ (Table 3). We performed this calculation by simply assuming that no spillover effect was taking place. At low conversions (catalytic tests performed at 200 °C), apparent TOF values reach 84 and 52 g^{-1}·h^{-1}, respectively, for 1%Ru_200 °C and 1%Ru_250 °C. Such values are in the same range for the two samples and are comparable to Ru systems with similar concentrations prepared by impregnation on the TiO_2[53] support and on a commercial reference Ru/Al_2O_3 reported in the literature.[54] Calculated TOF values of catalytic tests performed at 200 °C for 3%Ru_200 °C reach 359 g^{-1}·h^{-1} and 412 h^{-1} for the 3% Ru_250 °C sample. Reckoning that Ru NP size depends on the reduction temperature, the fact that the apparent TOF tends to differ may be related to the structure-sensitivity of this catalytic reaction.[55]

The catalytic performances of the 1% Ru/Al molar ratio prepared by the direct integrative one-pot solvent-free synthesis were compared to a reference Ru/Al_2O_3. This reference, named 1%Ru_Imp_Ref, was prepared by wetness impregnation of a preformed γ-Al_2O_3 support, which was made

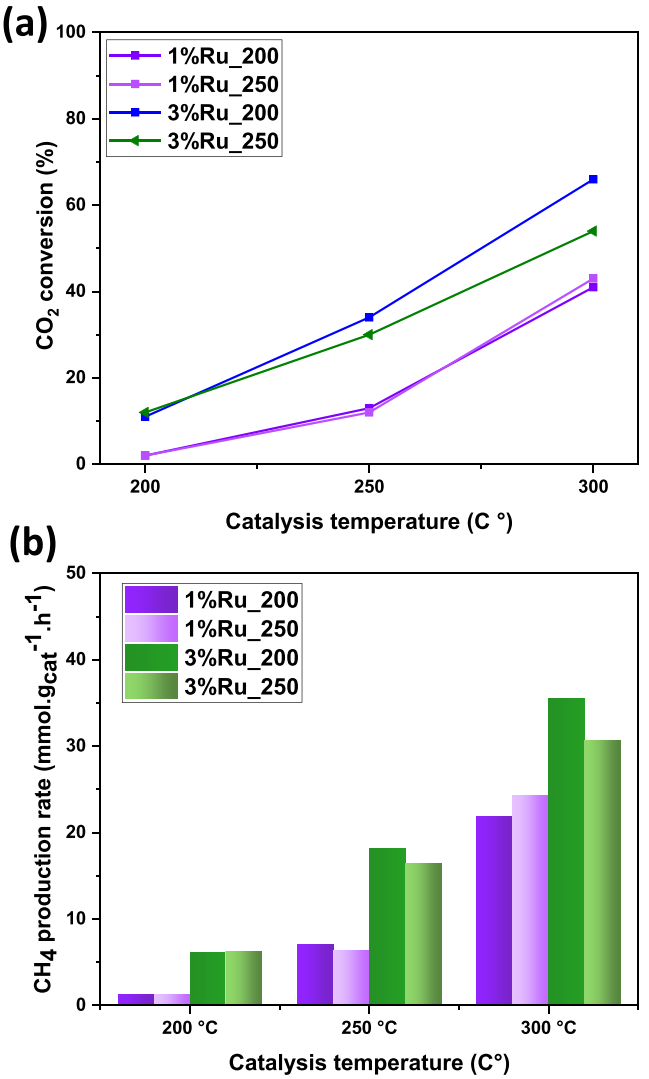

Figure 4. Catalytic performances at 200, 250, and 300 °C of the reduced samples prepared by the solvent-free synthesis method: (a) CO_2 conversion and (b) CH_4 production rate.

Table 3. Catalytic Performances of the Reduced Materials for the Hydrogenation of CO_2 to Methane[a]

sample	catalysis T (°C)	CO_2 conversion (%)	CH_4 production rate (mmol·g_{cat}^{-1}·h^{-1})	TOF (h^{-1})
	200	2	1.3	84
1%Ru200 °C	250	13	7.0	466
	300	41	21.9	1462
	200	2	1.2	52
1%Ru_250 °C	250	12	6.3	264
	300	43	24.3	1026
	200	2	0.9	
1%Ru_Imp-ref	250	10	5.7	
	300	43	25.9	
	200	11	6.1	359
3%Ru_200 °C	250	34	18.2	1072
	300	66	35.5	2092
	200	12	6.2	412
3%Ru_250 °C	250	30	16.4	1097
	300	54	30.6	2049

[a]In all experiments, we obtained a 100% selectivity for CH_4.

by solvent-free synthesis (S_{BET} = 393 $m^2 \cdot g^{-1}$ and V_p = 1.4 $cm^3 \cdot g$). Its final molar Ru/Al ratio was 1% (corresponding to 2 wt % %Ru/Al_2O_3). The XRD pattern and TEM images of γ-Al_2O_3 ref 1%Ru_Imp_Ref are presented in Figures S9 and S10, respectively. γ-Al_2O_3 was selected as it is a stable and very common heterogeneous catalyst support. In Figure 5, the three

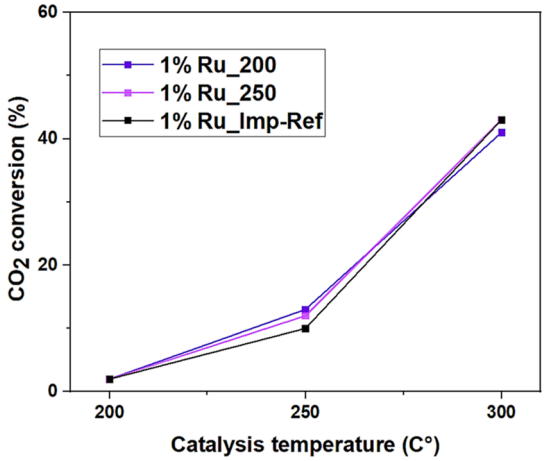

Figure 5. Catalytic activity of the 1% Ru/Al molar ratio samples prepared by direct one-step solvent-free synthesis catalysts and the reference prepared by wetness impregnation.

catalysts, 1%Ru_200 °C, 1%Ru_250 °C, and 1%Ru_Imp_Ref, exhibit very similar CO_2 methanation activity. Thus, the direct solvent-free, one-pot synthesis produces catalysts as efficient as impregnation.

In order to gather more information on the structural stability of our catalysts, the materials were characterized by XPS and TEM (Figure 6) after catalysis (that is, after 300 °C for 1 h). On TEM images, one can observe a larger Ru particle size distribution (Figure S11) after a catalytic test. XRD analyses of 3%Ru_200 °C and 3%Ru_250 °C after catalysis (Figure 6b) indicate a sharpening of the peak at 44° of the metallic Ru(101), which could be attributed to the sintering of Ru NPs during catalysis. From XPS (Figure 6a) of reduced 1% Ru_200 °C, 1%Ru_250 °C, and 3%Ru_250 °C samples, one observes a decrease in the Ru/Al ratio, which can be explained by the small photoelectron mean free path that promotes limited information depth on Ru(0) particles (some Ru centers cannot be detected anymore) (Table S2).

The solvent-free direct synthesis materials presented here display catalytic activity for CO_2 methanation, but their performance is still far from optimal. From the data gathered so far, we know that the solvent-free synthesis approach leads to mixed oxide structures in which Ru centers are very well dispersed. The reduction of the catalysts leads to the exsolution of ruthenium, one part of which is reduced. From TEM pictures and XRD, we clearly proved the presence of NPs in the range of 1 and 4 nm before catalytic tests, but considering their formation mechanism (exsolution), we cannot exclude the presence of single atoms and/or clusters of Ru(0). In the future, it will be necessary to determine the exact distribution of Ru centers within such a matrix and its evolution during the reduction step, heating, and catalytic tests. The objective is to optimize the thermal activation treatments of the mixed catalyst to improve the accessibility of ruthenium by adding phases (TiO_2) that can stabilize Ru on the surface. It would also be interesting to consider working with less expensive active phases, such as nickel.

However, from a sustainability point of view, as discussed in our previous article,[36] the synthesis process of the catalysts prepared by direct solvent-free sol−gel synthesis seems to be more efficient in terms of integration of the synthesis process compared to catalysts prepared by impregnation of the active phase on gamma-alumina prepared in the same conditions.

2.4. Atoms, Energy, and Liquid Waste Production Metrics. We made an attempt to compare the production of the Ru(0)/γ-AlOOH catalyst prepared by the solvent-free sol−gel method with the production of a classical Ru(0)/γ-Al_2O_3 catalyst prepared in a conventional way by precipitation of boehmite, calcination, and postimpregnation (which is representative of industrial reality).[36,56] We are aware that both catalysts do not have similar crystalline structures, but references to catalysts Ru(0)/γ-AlOOH are very hard to find in the literature. For the calculation of atoms and energy consumption, this difference has a limited effect (the additional calcination step will be specifically highlighted and discussed in order to avoid possible confusions).

We considered, in this section, three key indicators: atom consumption, energy consumption, and waste generation. To assess waste generation, we utilized two metrics: "E-factor", which is the total mass of waste divided by the produced mass of catalyst, not taking into consideration water, and "complete E-factor" or cE-factor which is the total mass of waste divided by the produced mass of catalyst, which considers water consumption as well (nowadays much more relevant according to the United Nations Challenges for this century).[57] Considering that water purification for synthesis is expensive and that recycling water consumes time and energy, the cE-factor provides a more relevant measure for assessing the environmental impact of the catalyst production process. We excluded from this evaluation all catalyst shaping steps because a vast majority of literature reports only the test of powder materials with no description of the shaping protocol. The energy consumption of the devices was not considered. As a consequence, we are comparatively estimating in this manuscript only the absolute minimum of energy needed for phase transitions, heating of solvents or solids, and evaporation processes. The exact estimation of industrial energetic cost requires a dedicated study, and the result depends mostly on the size of production units, the exact preparation protocols of industrial products, the type of production devices, and a proper multiplicative factor taking into consideration all thermal losses from heating and calcination steps. These data are not often shared by the industry, making it challenging to provide an exact estimation of the energetic cost without conducting a dedicated life cycle study. For a simple comparative study, we can simply consider that energetic consumption increases with the number of synthesis steps, the number of heating steps, and the volume of solvent used.

Two production scenarios were compared. First, a classical batch production method whose parameters have been taken from literature, including calcination steps, was chosen as a standard protocol.[14,55,58] It was already used as a reference in a previous article, which contains more details.[36] In this scenario, both acidic and basic aluminum salts are coprecipitated and aged in hot water to form γ-AlOOH. The as-obtained boehmite is then filtered and washed several times for removing counterions before drying. In that case, we considered the use of 0.75 $mol \cdot L^{-1}$ of aluminum salt in

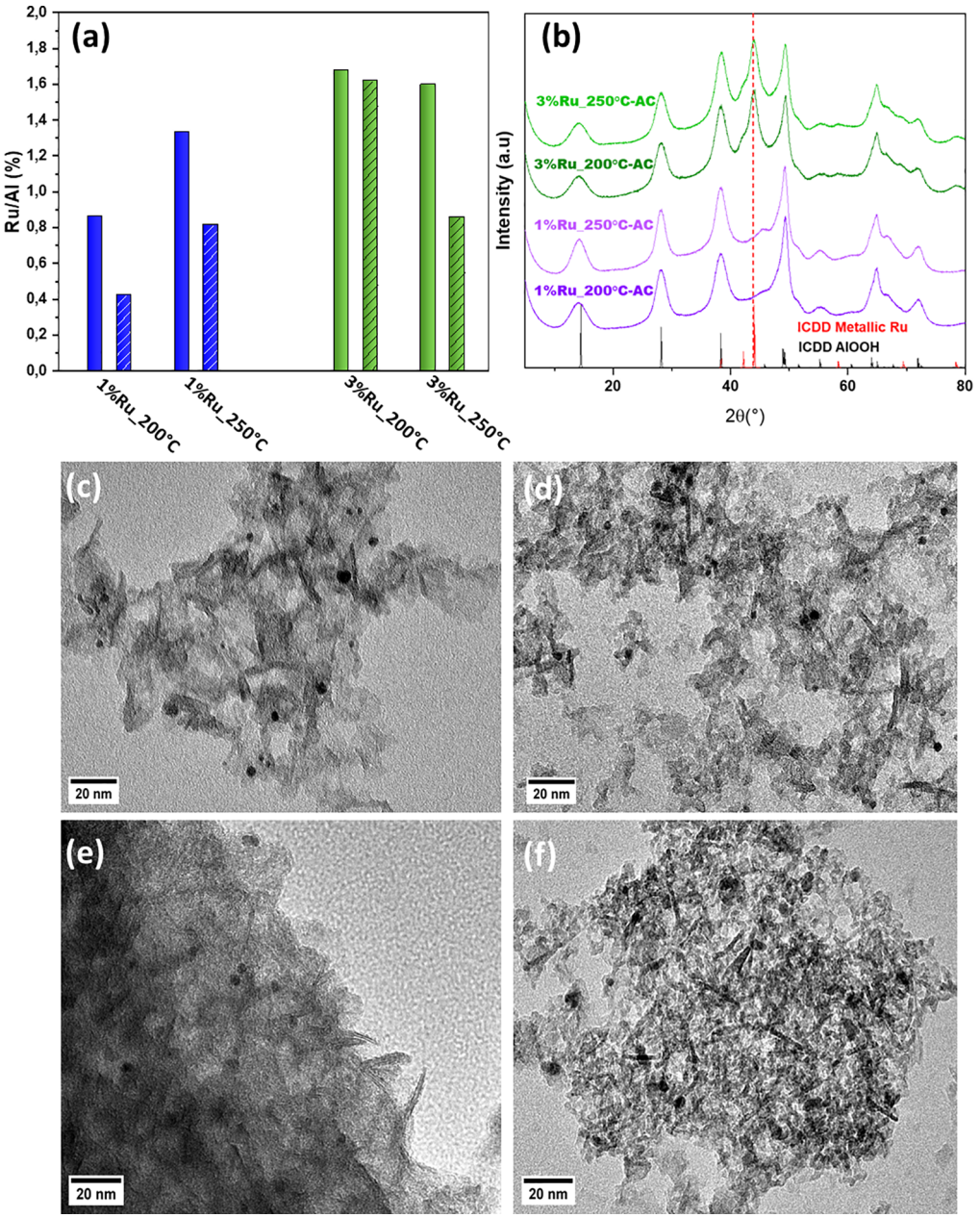

Figure 6. (a) Evolution of the XPS Ru/Al atomic ratio for the reduced samples before catalysis (filled bars) and after catalysis (hatched bars). (b) XRD patterns of 1%Ru_200 °C, 1%Ru_250 °C, 3%Ru_200 °C, and 3%Ru_250 °C after catalysis (AC stands for After catalysis) (c)TEM of 1% Ru_200 °C after catalysis, (d) TEM of 1%Ru_250 °C after catalysis, (e) TEM of 3%Ru_200 °C after catalysis, and (f) TEM of 3%Ru_250 °C after catalysis.

water and two possible precipitation temperatures, 30 and 85 °C. Regarding the washing step, we assumed that three times the volume of solvent used in the reaction is required at ambient temperature. Although this step is typically not extensively described in the literature, based on salt dilution calculations, it is likely that a minimum of three washings are necessary. After the last filtration and drying, boehmite is calcined to obtain porous γ-Al_2O_3. This powder is then impregnated with a $Ru(NO)(NO_3)_3$ precursor solution and dried (we used the strict minimum amount of water that is equal to 1.2 times the mesoporous volume of alumina powder). According to the literature, reaching the active phase loading of 2 wt % requires two successive impregnation steps.[55] Higher loadings require additional impregnation and evaporation steps (thus more atoms and more energy). The two final steps of the synthesis are a first calcination in air at 400 °C for decomposing the ruthenium precursor into the catalytic reactor and a second one under H_2 gas for the final conditioning, in which RuO_2 is reduced to Ru(0). For the latter, we assumed a temperature of 250 °C and very optimistically considered that there is no loss of H_2 during the process and only two H_2 molecules are enough for reducing a Ru(IV) center in Ru(0).

The second scenario is the as-proposed solvent-free reaction in which both aluminum alkoxide and $Ru(acac)_3$ precursors are first reacted at 130 °C (without any other reagents or solvents). In this scenario, we consider that the obtained reactant mixture is allowed to cool until 50 °C, the

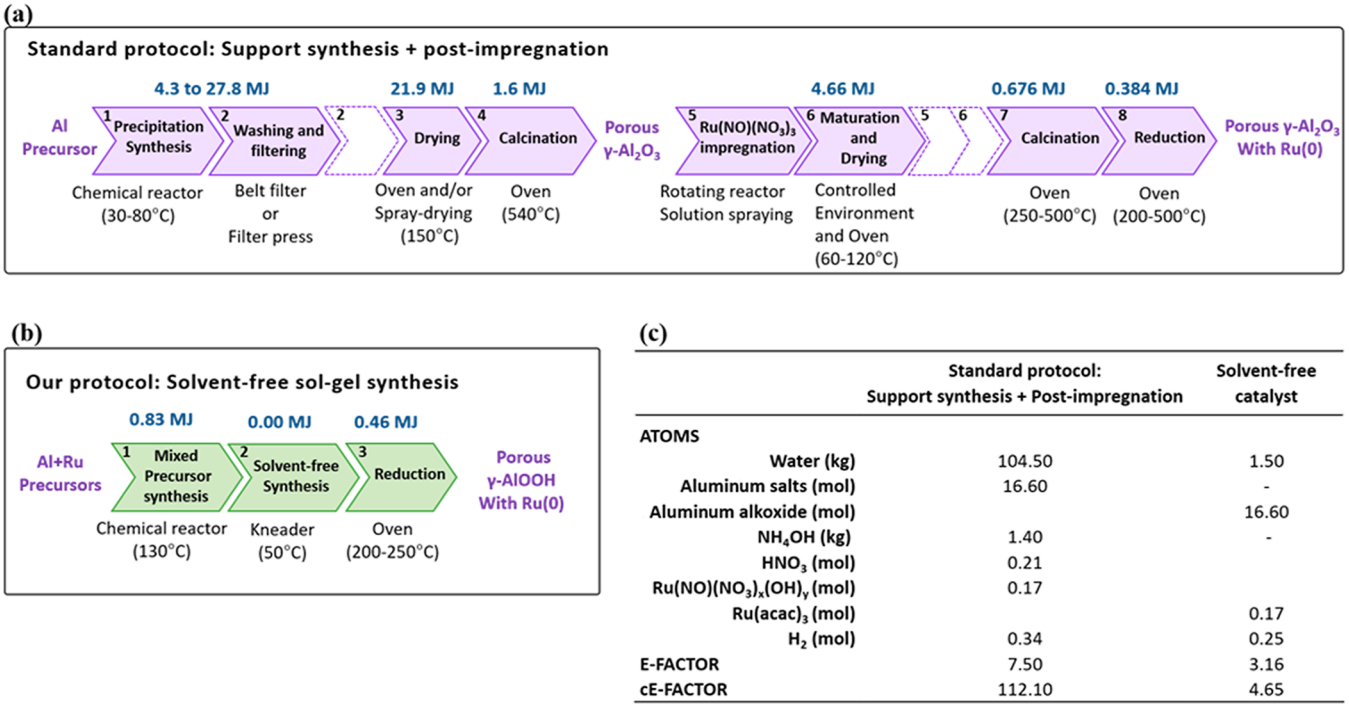

(c)

	Standard protocol: Support synthesis + Post-impregnation	Solvent-free catalyst
ATOMS		
Water (kg)	104.50	1.50
Aluminum salts (mol)	16.60	-
Aluminum alkoxide (mol)		16.60
NH_4OH (kg)	1.40	-
HNO_3 (mol)	0.21	
$Ru(NO)(NO_3)_x(OH)_y$ (mol)	0.17	
$Ru(acac)_3$ (mol)		0.17
H_2 (mol)	0.34	0.25
E-FACTOR	7.50	3.16
cE-FACTOR	112.10	4.65

Figure 7. Energy, atoms, and waste metrics given for the synthesis of 1 kg of AlOOH. The minimal energetic consumption of each synthesis step is written in blue (a) standard precipitation synthesis and incipient wetness impregnation protocols of support $Ru(0)/Al_2O_3$ catalysts. (b) Solvent-free sol−gel protocol of supported Ru(0)/AlOOH. (c) Atom, E-Factor, and cE-factor calculated for a conventional (precipitation + post impregnation) synthesis and our solvent-free synthesis.

temperature at which the small amount of water is introduced for the hydrolysis reaction. This reaction is exothermic, so no additional energy input is required for the 10 min of reaction. Although the exothermicity of this reaction is sufficient to evaporate the vast majority of the alcohol produced during the reaction, we considered that all of the alcohol produced required energy for its evaporation (we therefore assumed the worst possible energy consumption for our material). No calcination step is required for our material since the final conditioning, in which the Ru precursor is reduced to Ru(0) with H_2 gas, takes place in the catalytic reactor (it is performed at the same temperature as the first scenario at a temperature of 250 °C). In that case, we assume for calculations that Ru(III) is reduced to Ru(0).

All powder drying energy consumptions were calculated by considering only the vaporization enthalpies of species such as solvent or alcohol molecules. For example, the wet cake of boehmite typically contains between 84 and 93 wt % of water before drying[59,60] We summarized the comparison in Figure 7.

The comparison of water consumption between classic precipitation and solvent-free methods instantly emphasizes the significant advantage of direct solvent-free synthesis, which completely eliminates the need for solvents (using 69 times less water) and produces no liquid waste. When water is excluded from the calculation, the E-factor for the standard impregnation method is 2.4 times higher. A more realistic comparison based on cE-factors reveals a value of 112.1 for scenario 1, which is more than 24 times higher than that of the one-pot solvent-free method, highlighting the substantial sustainability benefit attainable through this frugal process.

Energy consumption for each step of the synthesis protocols of both scenarios (Figure 7a,b in blue) is given for the production of 1 kg of AlOOH. We can clearly see that conventional solution synthesis is by far the most energy-intensive due to the large amount of solvent and drying steps required for substrate preparation (synthesis, drying, and calcination) and impregnation (ripening and drying, calcination, and reduction). In contrast, the solvent-free sol−gel method consumes a very low amount of energy, 1.29 MJ/kg, while the standard protocol needs between 32.7 and 56.23 MJ/kg, (25−43 times more). If we compare scenarios at thet equivalent inorganic phase (boehmite), we can remove the contribution of step 4 of scenario 1 (calcination transforming boehmite into gamma alumina): the solvent-free scenario still consumes from 24 to 42 times less energy.

Although aluminum alkoxides are more expensive than their salt counterparts, it is very likely that the difference in reagent costs can be offset by the substantial savings in energy costs, waste management costs, and the reduction in the number of synthesis steps (reduction in the number of devices leading to lower investment, maintenance, and labor costs). Globally, the solvent-free sol−gel synthesis involves three steps and only one reactor in an easy way, which offers a realistic alternative to the impregnation multistep method. By eliminating the need for multiple steps and devices, this approach presents a global environmental footprint that is significantly improved.

3. CONCLUSIONS

The potential of a new solvent-free synthesis strategy for preparing $Ru(0)/\gamma$-AlOOH and $Ru(0)/\gamma$-Al_2O_3 supported ruthenium catalysts for CO_2 methanation was investigated. We first developed a direct integrative solvent-free preparation of mixed Al/Ru mixed oxide by sol−gel co-condensation of ASB and $Ru(acac)_3$ precursor, leading, after reduction, to a very efficient dispersion of Ru centers (NPs from 1 to 4 nm) within a high surface area AlOOH matrix. We compared the

catalytic properties of co-condensed materials and post-impregnated ones and observed that both types presented similar and interesting catalytic performances (considering that a significant part of Ru is not accessible to H_2 chimisorption). We demonstrate with this work that it is possible to synthesize efficient and competitively supported catalysts with a minimalist process. This proof-of-concept allows us to take a step toward frugal innovation in the preparation of supported catalysts that focus on providing essential functionalities by eliminating nonessential features and components with a drastic atom and energy economy. By extension, our approach is easy to extend to numerous mixed oxide compositions (coming paper) adapted to various catalytic reactions. We believe that this approach, which drastically reduces complexity, is very promising, for it can achieve highly integrated industrial processing requiring a very low amount of energy using a strict minimum of atoms and producing almost no waste.

4. EXPERIMENTAL SECTION

4.1. Materials. Ruthenium(III) acetylacetonate and aluminum trisec-butoxide were purchased from Sigma-Aldrich. Ruthenium(III) nitrosyl nitrate, 1.5% w/v in a diluted aq. nitric acid solution, was purchased from Thermo Scientific Chemicals. All chemicals were used as received without further purification.

4.2. Preparation of Ru-Based Catalysts. The solvent-free sol–gel synthesis of the Ru-based catalysts was performed as follows: $Ru(acac)_3$ is mixed with aluminum trisec-butoxide (ASB) with Ru/Al molar ratios of 1 and 3% (equivalent to wt %Ru 2% Ru/Al_2O_3 and 6% Ru/Al_2O_3) without the addition of solvent. The reactive medium is then aged at 130 °C for 8 h in an oven in order to have a homogeneous mixture. Then, it is hydrolyzed in a mixer with a steel anchor for 10 min at 210 tr·min^{-1}, with a hydrolysis ratio h = 5.

Gels resulting from the synthesis were dried for 12 h under a vacuum at 25 °C to obtain powders. They are labeled as "pristine" materials. These powders were then reduced at 200 and 250 °C under pure H_2 at 2 bar in static conditions for 4 h before being tested for CO_2 methanation.

Reference Ru/Al_2O_3 materials were prepared by incipient wetness impregnation of solvent free-sol–gel Al_2O_3 (prepared according to ref 36)[36] with Ruthenium(III) nitrosyl nitrate solution concentrated at 1.5% (typical). Two Ru loading Ru/Al molar ratios of 1 and 3% (equivalent to wt %Ru 2% Ru/Al_2O_3 and 6% Ru/Al_2O_3) were prepared. These powders were dried under a vacuum at 40 °C before being reduced at 250 °C under pure H_2 at 2 bar for 4 h. The obtained catalyst is labeled 1%Ru_Imp-ref.

4.3. Reactive Media Characterization. *4.3.1. NMR.* NMR spectroscopy experiments were performed on a Bruker AV^{III} 300 spectrometer, operating at 300.13 and 78.21 MHz for ^{1}H and ^{27}Al, respectively, and equipped with a 5 mm BBFO probe. The samples were diluted in $CDCl_3$ prior to analysis. ^{27}Al chemical shifts are referenced to an external $Al(NO_3)_3$ 1 M solution in D_2O. The probe signal was subtracted from the ^{27}Al spectra. ^{1}H chemical shifts are internally referenced using the protonated impurity of the solvent, $d(CHCl_3/CDCl_3)$ = 7.26 ppm. The deconvolution of the ^{27}Al NMR spectra was carried out with DMFit software.[61]

4.4. Catalyst Characterizations (Powders). *4.4.1. Energy Dispersive X-ray Fluorescence.* Elemental analyses of the powders were carried out by EDXRF using an Epsilon 3XL spectrometer from Malvern-Panalytical equipped with a silver X-ray tube. The calibration was performed by depositing a mass in the range 0–20 μg of the standard solution of each element with a concentration of about 1 g·L^{-1} on a polycarbonate membrane. The detection limit for Ru was determined to be 25.9 ng.

4.4.2. X-ray Diffraction. X-ray diffraction (XRD) was carried out by a low-angle diffractometer, Bragg–Brentano Bruker D8 ADVANCE, using filtered Cu Kα radiation over a 2θ range of 4 to 80° with a step size of 0.02°.

4.4.3. Transmission Electron Microscopy. Transmission electron microscopy (TEM) was carried out by a TECNAI 120 Spirit Twin instrument at an acceleration voltage of 120.0 kV with a Gatan Orius 1000 camera model.

4.4.4. STEM–EDX and HAADF. STEM/EDX characterizations were performed on a JEOL 2100 Plus microscope equipped with a LaB_6 gun. Mapping and EDX of the O, Al, and Ru elements were collected by combining HAADF-STEM (high angular annular dark field scanning transmission electron microscopy) and an EDX Oxford detector (SDD 80 mm^2, Oxford Aztec software).

4.4.5. XPS. XPS analyses were performed using an Argus X-ray photoelectron spectrometer equipped with a monochromated Al Kα radiation source ($h\nu$ = 1486.6 eV) and a 280 W electron beam power. The emission of photoelectrons from the sample was analyzed at a takeoff angle of 45° under ultrahigh vacuum conditions (≤10–9 mbar). Spectra were carried out with a 100 eV pass energy for the survey scan and a 20 eV pass energy for the core-level regions. Binding energies were calibrated against the C 1s (C–C) binding energy at 284.8 eV, and element peak intensities were corrected by Scofield factors. The peak areas were determined after subtraction of a *U 2 TOUGAARD* background. The spectra were fitted using Casa XPS v.2.3.15 software (Casa Software Ltd., U.K.) and applying a Gaussian/Lorentzian ratio g/l equal to 70/30.

4.4.6. Nitrogen Adsorption–Desorption Analysis. The specific surface area of the catalysts was obtained by the nitrogen adsorption–desorption isotherm collected at 77 K on a BELSORP Max from MicrotracBEL. The samples were outgassed for 6 h at 110 °C prior to the analysis. S_{BET} was calculated by applying the BET method for N2 relative pressure in a range of $0.05 < P/P_0 < 0.35$, and the pore size distribution was estimated by Barrett–Joyner–Halenda (BJH) method[62] on the desorption data.

4.4.7. H_2 Chemisorption. The accessible Ru atoms on the catalyst surface were evaluated by H_2 chemisorption at 35 °C using a 3Flex apparatus from Micrometrics. Catalysts reduced under pure H_2 at 200 and 250 °C with weights between 100 and 230 mg were analyzed. They were introduced into a Pyrex tube and secured with quartz fibers. They were first degassed under a vacuum at 80 °C for 30 min, with a temperature rate of 3 °C/min to reach 80 °C, followed by a treatment under He at 110 °C for 1 h and an adsorption of H_2. Two isotherms were measured in the range of 0.13–60 kPa. The first isotherm corresponds to reversible physisorption and irreversible chemisorption. The sample was then evacuated, and the adsorbed H_2 was reversibly desorbed to measure the second isotherm corresponding to the physisorbed H_2. The linear part of the two isotherms was subtracted to get the total amount of irreversibly adsorbed H_2, which stands for the chemisorbed H_2. The metal dispersion, $Ru_{surface}/Ru_{bulk}$, is estimated from a hydrogen adsorbed on Ru bulk (Had/Rubulk) ratio assuming a chemisorption stoichiometry H/Ru = 1 for all the samples.

4.4.8. Catalytic Activity Measurement. The catalytic performances of the reduced materials prepared by direct solvent-free synthesis and the references prepared by wetness impregnation were measured in a continuous-flow gas-phase reactor at atmospheric pressure. For each test, 100 mg of undiluted catalyst was introduced inside a stainless-steel flow reactor (without any pelletizing, grinding, or sieving) and secured with quartz fiber wool. The catalyst was preactivated in situ for 2 h under H_2 30 mL·min^{-1} at 200 °C with a 5 °C·min^{-1} temperature rate to reach the plateau. For the catalytic test, a mixture corresponding to a stoichiometric feed of (H_2/CO_2/He) (1:4:5) was injected. The gas hourly space velocity of the mixture gas was 12,000 mL·g^{-1}·h^{-1}. The catalytic activity and selectivity were measured while sweeping the reaction temperature at 200, 250, and 300 °C using a 5 °C/min ramp rate between temperature points. The temperature was kept for 2 h at each point to reach the stable state, indicated by at least consecutively stable effluent gas measurements. A thermocouple located inside the catalyst bed was used to measure the real temperature inside the reactor. The products from CO_2 methanation were analyzed online with a Shimadzu gas chromatograph GC2014 equipped with both a thermal conductivity detector (TCD) and a flame ionization detector. The CO_2 conversion (X_{CO_2}) and intrinsic

turnover frequency (TOF) were calculated according to the equations below, where F is the molar flow rate, N_{Ru} is the mole of Ru surface atom calculated from H_2 chemisorption normalized on sample weight, and CH_4 selectivity is 100%

$$X_{CO2}(\%) = \frac{F_{CO2,in} - F_{CO2,out}}{F_{CO2,in}} \quad (1)$$

$$TOF(h^{-1}) = \frac{X_{CO2} \times F_{CO2,in}}{NRu_{Surf}} \quad (2)$$

■ ASSOCIATED CONTENT

Supporting Information

The Supporting Information is available free of charge at https://pubs.acs.org/doi/10.1021/acs.chemmater.3c01746.

^{27}Al NMR and ^{1}H NMR spectra for all compounds, isotherms and the pore size distribution for samples analyzed by N_2 physisorption analysis, XPS results and the associated analysis of the catalysts before and post CO_2 methanation catalysis, powder X-ray diffraction patterns and TEM of the references prepared by impregnation, and particle size distributions determined by TEM for the catalysts before and post CO_2 methanation catalysis (PDF)

STEM tomography of the 3%Ru_250 °C catalyst (AVI)

■ AUTHOR INFORMATION

Corresponding Authors

Corinne Chaneac − *Collège de France, Laboratoire de Chimie de la Matière Condensée de Paris (LCMCP), Sorbonne Université, CNRS, 75005 Paris, France;* orcid.org/0000-0001-9785-1052; Email: corinne.chaneac@upmc.fr

Cédric Boissière − *Collège de France, Laboratoire de Chimie de la Matière Condensée de Paris (LCMCP), Sorbonne Université, CNRS, 75005 Paris, France;* orcid.org/0000-0003-1212-6850; Email: cedric.boissiere@sorbonne-universite.fr

Authors

Ryma Haddad − *Collège de France, Laboratoire de Chimie de la Matière Condensée de Paris (LCMCP), Sorbonne Université, CNRS, 75005 Paris, France*

Yingrui Zhao − *Institute of Condensed Matter and Nanosciences (IMCN), Université catholique de Louvain (UCLouvain), Louvain-La-Neuve 1348, Belgium*

Antoine Miche − *Fédération de Chimie et Matériaux de Paris-Centre (FCMat) and Laboratoire de Réactivité de Surface (LRS), Sorbonne Université, CNRS, Paris 75005, France*

Ferdaous Ben Romdhane − *Fédération de Chimie et Matériaux de Paris-Centre (FCMat) and Laboratoire de Réactivité de Surface (LRS), Sorbonne Université, CNRS, Paris 75005, France*

Nivedita Sudheer − *France Institut de Physique et de Chimie des Matériaux de Strasbourg (IPCMS), Université de Strasbourg-CNRS, Strasbourg 67200, France*

Ovidiu Ersen − *France Institut de Physique et de Chimie des Matériaux de Strasbourg (IPCMS), Université de Strasbourg-CNRS, Strasbourg 67200, France;* orcid.org/0000-0002-1553-0915

François Devred − *Institute of Condensed Matter and Nanosciences (IMCN), Université catholique de Louvain (UCLouvain), Louvain-La-Neuve 1348, Belgium*

François Ribot − *Collège de France, Laboratoire de Chimie de la Matière Condensée de Paris (LCMCP), Sorbonne Université, CNRS, 75005 Paris, France;* orcid.org/0000-0001-5576-7725

Capucine Sassoye − *Collège de France, Laboratoire de Chimie de la Matière Condensée de Paris (LCMCP), Sorbonne Université, CNRS, 75005 Paris, France;* orcid.org/0000-0003-2790-888X

Clement Sanchez − *Collège de France, Laboratoire de Chimie de la Matière Condensée de Paris (LCMCP), Sorbonne Université, CNRS, 75005 Paris, France;* orcid.org/0000-0002-6426-4844

Damien P. Debecker − *Institute of Condensed Matter and Nanosciences (IMCN), Université catholique de Louvain (UCLouvain), Louvain-La-Neuve 1348, Belgium;* orcid.org/0000-0001-6500-2996

Complete contact information is available at:

Author Contributions

The manuscript was written through the contributions of all authors. All authors have given approval to the final version of the manuscript. R.H. performed materials synthesis, characterizations, data treatments, bibliographic studies, and manuscript writing; Y.Z. performed catalytic test experiments; A.M. performed XPS analysis and data treatments; Ferdaous Benromdhane, performed HRTEM and STEM analysis; N.S. performed STEM tomography analysis; O.E. provided expertise in STEM tomography analysis; F.R. performed NMR (^{27}Al and ^{1}H) analysis, data treatment, and interpreta-tion and manuscript writing; C.S. provided expertise in conventional sol−gel synthesis of Ru-base catalysts; D.P.D. performed catalytic studies on conception and interpretation, management, and manuscript writing; C.S. performed and conceived the study and scientific discussion; C.C. performed and conceived the study, student management, data interpretation, and manuscript writing; and C.B. performed and conceived the study, student management, data interpretation, and manuscript writing.

Funding

This work was supported by ED397 Doctoral School Materials Physics/Chemistry of Sorbonne University.

Notes

The authors declare no competing financial interest.

■ ACKNOWLEDGMENTS

Sophie Nowak, the person in charge of the X-ray plateform of Université Paris Cité, is gratefully acknowledged for the help in conducting EDXRF analysis.

■ REFERENCES

(1) Chen, T.-L.; Kim, H.; Pan, S.-Y.; Tseng, P.-C.; Lin, Y.-P.; Chiang, P.-C. Implementation of Green Chemistry Principles in Circular Economy System towards Sustainable Development Goals: Challenges and Perspectives. *Sci. Total Environ.* **2020**, *716*, 136998.

(2) 12 Principles of Green Chemistry. American Chemical Society. https://www.acs.org/greenchemistry/principles/12-principles-of-green-chemistry.html (accessed Mar 16, 2023).

(3) Ananikov, V. P.; Khemchyan, L. L.; Ivanova, Y. V.; Bukhtiyarov, V. I.; Sorokin, A. M.; Prosvirin, I. P.; Vatsadze, S. Z.; Medved'ko, A. V.; Nuriev, V. N.; Dilman, A. D.; Levin, V. V.; Koptyug, I. V.; Kovtunov, K. V.; Zhivonitko, V. V.; Likholobov, V. A.; Romanenko, A. V.; Simonov, P. A.; Nenajdenko, V. G.; Shmatova, O. I.;

Muzalevskiy, V. M.; Nechaev, M. S.; Asachenko, A. F.; Morozov, O. S.; Dzhevakov, P. B.; Osipov, S. N.; Vorobyeva, D. V.; Topchiy, M. A.; Zotova, M. A.; Ponomarenko, S. A.; Borshchev, O. V.; Luponosov, Y. N.; Rempel, A. A.; Valeeva, A. A.; Stakheev, A. Y.; Turova, O. V.; Mashkovsky, I. S.; Sysolyatin, S. V.; Malykhin, V. V.; Bukhtiyarova, G. A.; Terent'ev, A. O.; Krylov, I. B. Development of New Methods in Modern Selective Organic Synthesis: Preparation of Functionalized Molecules with Atomic Precision. *Russ. Chem. Rev.* **2014**, *83* (10), 885−985.

(4) Espro, C.; Paone, E.; Mauriello, F.; Gotti, R.; Uliassi, E.; Bolognesi, M. L.; Rodríguez-Padrón, D.; Luque, R. Sustainable Production of Pharmaceutical, Nutraceutical and Bioactive Compounds from Biomass and Waste. *Chem. Soc. Rev.* **2021**, *50* (20), 11191−11207.

(5) Fechete, I.; Wang, Y.; Védrine, J. C. The Past, Present and Future of Heterogeneous Catalysis. *Catal. Today* **2012**, *189* (1), 2−27.

(6) Olivos-Suarez, A. I.; Szécsényi, À.; Hensen, E. J. M.; Ruiz-Martinez, J.; Pidko, E. A.; Gascon, J. Strategies for the Direct Catalytic Valorization of Methane Using Heterogeneous Catalysis: Challenges and Opportunities. *ACS Catal.* **2016**, *6* (5), 2965−2981.

(7) Glotov, A.; Karakhanov, E. Heterogeneous Catalysts for Petrochemical Synthesis and Oil Refining. *Catalysts* **2021**, *11* (5), 602.

(8) Kim, A.; Debecker, D. P.; Devred, F.; Dubois, V.; Sanchez, C.; Sassoye, C. CO2 Methanation on Ru/TiO2 Catalysts: On the Effect of Mixing Anatase and Rutile TiO2 Supports. *Appl. Catal., B* **2018**, *220*, 615−625.

(9) Tang, Z.-E.; Lim, S.; Pang, Y.-L.; Ong, H.-C.; Lee, K.-T. Synthesis of Biomass as Heterogeneous Catalyst for Application in Biodiesel Production: State of the Art and Fundamental Review. *Renew. Sustain. Energy Rev.* **2018**, *92*, 235−253.

(10) Hijazi, A.; Khalaf, N.; Kwapinski, W.; Leahy, J. J. Catalytic Valorisation of Biomass Levulinic Acid into Gamma Valerolactone Using Formic Acid as a H 2 Donor: A Critical Review. *RSC Adv.* **2022**, *12* (22), 13673−13694.

(11) Losfeld, G.; Escande, V.; Jaffré, T.; L'Huillier, L.; Grison, C. The Chemical Exploitation of Nickel Phytoextraction: An Environmental, Ecologic and Economic Opportunity for New Caledonia. *Chemosphere* **2012**, *89* (7), 907−910.

(12) Hu, X.; Yip, A. C. K. Heterogeneous Catalysis: Enabling a Sustainable Future. *Front. Catal.* **2021**, *1*, 667675.

(13) Tchenar, Y. N.; Choukchou-Braham, A.; Bachir, R. RuO2 Supported on V2O5-Al2O3 Material as Heterogeneous Catalyst for Cyclohexane Oxidation Reaction. *Bull. Mater. Sci.* **2012**, *35* (4), 673−681.

(14) Janke, C.; Duyar, M. S.; Hoskins, M.; Farrauto, R. Catalytic and Adsorption Studies for the Hydrogenation of CO2 to Methane. *Appl. Catal., B* **2014**, *152*−*153*, 184−191.

(15) Frontera, P.; Macario, A.; Ferraro, M.; Antonucci, P. Supported Catalysts for CO2 Methanation: A Review. *Catalysts* **2017**, *7* (2), 59.

(16) Yan, Y.; Wang, Q.; Jiang, C.; Yao, Y.; Lu, D.; Zheng, J.; Dai, Y.; Wang, H.; Yang, Y. Ru/Al2O3 Catalyzed CO2 Hydrogenation: Oxygen-Exchange on Metal-Support Interfaces. *J. Catal.* **2018**, *367*, 194−205.

(17) Guo, Y.; Mei, S.; Yuan, K.; Wang, D.-J.; Liu, H.-C.; Yan, C.-H.; Zhang, Y.-W. Low-Temperature CO2 Methanation over CeO2-Supported Ru Single Atoms, Nanoclusters, and Nanoparticles Competitively Tuned by Strong Metal-Support Interactions and H-Spillover Effect. *ACS Catal.* **2018**, *8* (7), 6203−6215.

(18) Munnik, P.; de Jongh, P. E.; de Jong, K. P. Recent Developments in the Synthesis of Supported Catalysts. *Chem. Rev.* **2015**, *115* (14), 6687−6718.

(19) Debecker, D. P.; Le Bras, S.; Boissière, C.; Chaumonnot, A.; Sanchez, C. Aerosol Processing: A Wind of Innovation in the Field of Advanced Heterogeneous Catalysts. *Chem. Soc. Rev.* **2018**, *47* (11), 4112−4155.

(20) Smith, S. J.; Amin, S.; Woodfield, B. F.; Boerio-Goates, J.; Campbell, B. J. Phase Progression of γ-Al2O3 Nanoparticles Synthesized in a Solvent-Deficient Environment. *Inorg. Chem.* **2013**, *52* (8), 4411−4423.

(21) Huang, B.; Bartholomew, C. H.; Smith, S. J.; Woodfield, B. F. Facile Solvent-Deficient Synthesis of Mesoporous γ-Alumina with Controlled Pore Structures. *Microporous Mesoporous Mater.* **2013**, *165*, 70−78.

(22) Huang, B.; Bartholomew, C. H.; Woodfield, B. F. Facile Structure-Controlled Synthesis of Mesoporous γ-Alumina: Effects of Alcohols in Precursor Formation and Calcination. *Microporous Mesoporous Mater.* **2013**, *177*, 37−46.

(23) Huang, B.; Bartholomew, C. H.; Woodfield, B. F. Facile Synthesis of Mesoporous γ-Alumina with Tunable Pore Size: The Effects of Water to Aluminum Molar Ratio in Hydrolysis of Aluminum Alkoxides. *Microporous Mesoporous Mater.* **2014**, *183*, 37−47.

(24) Smith, S. J.; Huang, B.; Liu, S.; Liu, Q.; Olsen, R. E.; Boerio-Goates, J.; Woodfield, B. F. Synthesis of Metal Oxide Nanoparticles via a Robust "Solvent-Deficient" Method. *Nanoscale* **2015**, *7* (1), 144−156.

(25) Oh, J.; Bathula, H. B.; Park, J. H.; Suh, Y.-W. A Sustainable Mesoporous Palladium-Alumina Catalyst for Efficient Hydrogen Release from N-Heterocyclic Liquid Organic Hydrogen Carriers. *Commun. Chem.* **2019**, *2* (1), 68.

(26) Kore, R. M.; Lokhande, B. J. A Robust Solvent Deficient Route Synthesis of Mesoporous Fe2O3 Nanoparticles as Supercapacitor Electrode Material with Improved Capacitive Performance. *J. Alloys Compd.* **2017**, *725*, 129−138.

(27) Woodfield, B. F.; Liu, S.; Boerio-Goates, J.; Liu, Q.; Smith, S. J. Preparation of Uniform Nanoparticles of Ultra-High Purity Metal Oxides, Mixed Metal Oxides, Metals, and Metal Alloys. US Patent 8,211,388 B2, July 3, 2012. https://patents.google.com/patent/US8211388B2/en?oq=US8211388 (accessed 2022−03−08).

(28) Zeljković, S. A Review of Recent Development of the Solvent-Deficient Method. *Contemp. Mater.* **2022**, *13* (2), 51−160.

(29) Park, S.; Kannapu, H. P. R.; Jeong, C.; Kim, J.; Suh, Y.-W. Highly Active Mesoporous Cu-Al2O3 Catalyst for the Hydrodeoxygenation of Furfural to 2-Methylfuran. *ChemCatChem* **2020**, *12* (1), 105−111.

(30) Smith, S. J.; Huang, B.; Bartholomew, C. H.; Campbell, B. J.; Boerio-Goates, J.; Woodfield, B. F. La-Dopant Location in La-Doped γ-Al2O3 Nanoparticles Synthesized Using a Novel One-Pot Process. *J. Phys. Chem. C* **2015**, *119* (44), 25053−25062.

(31) Reddy, K. H. P.; Kim, B.-S.; Lam, S. S.; Jung, S.-C.; Song, J.; Park, Y.-K. Effective Toluene Oxidation under Ozone over Mesoporous MnOx/γ-Al2O3 Catalyst Prepared by Solvent Deficient Method: Effect of Mn Precursors on Catalytic Activity. *Environ. Res.* **2021**, *195*, 110876.

(32) Lokhande, P. E.; Pawar, K.; Chavan, U. S. Chemically deposited ultrathin α-Ni(OH)2 nanosheet using surfactant on Ni foam for high performance supercapacitor application. *Mater. Sci. Energy Technol.* **2018**, *1* (2), 166−170.

(33) Kore, R. M.; Thakur, A. V.; Fugare, B. Y.; Lokhande, B. J. Reagent Ratio Dependent Physical Properties and Electrochemical Performance of NiO Nanoparticles Synthesized Using Solvent Deficient Approach. *AIP Conf. Proc.* **2018**, *1942* (1), 140069.

(34) Spencer, E. C.; Kolesnikov, A. I.; Woodfield, B. F.; Ross, N. L. New Insights about CuO Nanoparticles from Inelastic Neutron Scattering. *Nanomaterials* **2019**, *9* (3), 312.

(35) Kore, R. M.; Lokhande, B. J. Facile Solvent Deficient Synthesis of Mesoporous Co3O4 Nanoparticles for Electrochemical Energy Storage. *J. Mater. Sci.: Mater. Electron.* **2020**, *31* (8), 6174−6184.

(36) Dassie, P.-I.; Haddad, R.; Lenez, M.; Chaumonnot, A.; Boualleg, M.; Legriel, P.; Styskalik, A.; Haye, B.; Selmane, M.; Debecker, D. P.; Sanchez, C.; Chaneac, C.; Boissiere, C. Coupling of Solvent-Free Synthesis and Reactive Extrusion of Alumina: An Ecologically Efficient Integration for Heterogenous Catalyst Synthesis. *Green Chem.* **2023**, *25* (7), 2800−2814.

(37) Kříž, O.; Čásenský, B.; Lyčka, A.; Fusek, J.; Heřmánek, S. 27Al NMR Behavior of Aluminum Alkoxides. *J. Magn. Reson.* **1984**, *60* (3), 375−381.
(38) Tadanaga, K.; Minami, T.; Tohge, N. 27Al NMR Study of Coordination States of Aluminum-Tri-Sec-Butoxide Dissolved in Diacetone Alcohol. *Chem. Lett.* **1994**, *23* (8), 1507−1510.
(39) Babonneau, F.; Coury, L.; Livage, J. Aluminum Sec-Butoxide Modified with Ethylacetoacetate: An Attractive Precursor for the Sol-Gel Synthesis of Ceramics. *J. Non-Cryst. Solids* **1990**, *121* (1−3), 153−157.
(40) Bonhomme-Coury, L.; Babonneau, F.; Livage, J. Investigation of the Sol-Gel Chemistry of Ethylacetoacetate Modified Aluminum Sec-Butoxide. *J. Sol-Gel Sci. Technol.* **1994**, *3* (3), 157−168.
(41) Tadanaga, K.; Iwami, T.; Tohge, N.; Minami, T. Precursor Structure and Hydrolysis-Gelation Process of Al(O-Sec-Bu)3 Modified with Ethylacetoacetate. *J. Sol-Gel Sci. Technol.* **1994**, *3* (1), 5−10.
(42) Munery, S.; Ratel-Ramond, N.; Benjalal, Y.; Vernisse, L.; Guillermet, O.; Bouju, X.; Coratger, R.; Bonvoisin, J. Synthesis and Characterization of a Series of Ruthenium Tris(β-Diketonato) Complexes by an UHV-STM Investigation and Numerical Calculations. *Eur. J. Inorg. Chem.* **2011**, *2011* (17), 2698−2705.
(43) Pritchard, B.; Autschbach, J. Theoretical Investigation of Paramagnetic NMR Shifts in Transition Metal Acetylacetonato Complexes: Analysis of Signs, Magnitudes, and the Role of the Covalency of Ligand-Metal Bonding. *Inorg. Chem.* **2012**, *51* (15), 8340−8351.
(44) Oh, K.-T.; Kim, H.; Kim, D.; Han, J. H.; Park, J.; Park, J.-S. Facile Synthesis of AlOx Dielectrics via Mist-CVD Based on Aqueous Solutions. *Ceram. Int.* **2017**, *43* (12), 8932−8937.
(45) Ji, L.; Lin, J.; Tan, K. L.; Zeng, H. C. Synthesis of High-Surface-Area Alumina Using Aluminum Tri-Sec-Butoxide-2,4-Pentanedione-2-Propanol-Nitric Acid Precursors. *Chem. Mater.* **2000**, *12* (4), 931−939.
(46) Alphonse, P.; Courty, M. Structure and Thermal Behavior of Nanocrystalline Boehmite. *Thermochim. Acta* **2005**, *425* (1−2), 75−89.
(47) Zhu, H. Y.; Riches, J. D.; Barry, J. C. γ-Alumina Nanofibers Prepared from Aluminum Hydrate with Poly(Ethylene Oxide) Surfactant. *Chem. Mater.* **2002**, *14* (5), 2086−2093.
(48) Komaya, T.; Bell, A. T.; Wengsieh, Z.; Gronsky, R.; Engelke, F.; King, T. S.; Pruski, M. The Influence of Metal-Support Interactions on the Accurate Determination of Ru Dispersion for Ru/TiO2. *J. Catal.* **1994**, *149* (1), 142−148.
(49) Shen, X.; Garces, L.-J.; Ding, Y.; Laubernds, K.; Zerger, R. P.; Aindow, M.; Neth, E. J.; Suib, S. L. Behavior of H2 Chemisorption on Ru/TiO2 Surface and Its Application in Evaluation of Ru Particle Sizes Compared with TEM and XRD Analyses. *Appl. Catal., A* **2008**, *335* (2), 187−195.
(50) Gholampour, N.; Zhao, Y.; Devred, F.; Sassoye, C.; Casale, S.; Debecker, D. P. CO2 Methanation over Cobalt Nanoparticles Embedded in ZIF-L-Derived Porous Carbon. *ChemCatChem* **2023**, *15*, No. e202201338.
(51) Fu, L.; Zhou, J.; Zhou, L.; Yang, J.; Liu, Z.; Wu, K.; Zhao, H.; Wang, J.; Wu, K. Facile Fabrication of Exsolved Nanoparticle-Decorated Hollow Ferrite Fibers as Active Electrocatalyst for Oxygen Evolution Reaction. *Chem. Eng. J.* **2021**, *418*, 129422.
(52) Ashok, J.; Pati, S.; Hongmanorom, P.; Tianxi, Z.; Junmei, C.; Kawi, S. A Review of Recent Catalyst Advances in CO2 Methanation Processes. *Catal. Today* **2020**, *356*, 471−489.
(53) Kim, A.; Sanchez, C.; Patriarche, G.; Ersen, O.; Moldovan, S.; Wisnet, A.; Sassoye, C.; Debecker, D. P. Selective CO2 Methanation on Ru/TiO2 Catalysts: Unravelling the Decisive Role of the TiO2 Support Crystal Structure. *Catal. Sci. Technol.* **2016**, *6* (22), 8117−8128.
(54) Garbarino, G.; Bellotti, D.; Finocchio, E.; Magistri, L.; Busca, G. Methanation of Carbon Dioxide on Ru/Al2O3: Catalytic Activity and Infrared Study. *Catal. Today* **2016**, *277*, 21−28.
(55) Quindimil, A.; Bacariza, M. C.; González-Marcos, J. A.; Henriques, C.; González-Velasco, J. R. Enhancing the CO2 Methanation Activity of γ-Al2O3 Supported Mono- and Bi-Metallic Catalysts Prepared by Glycerol Assisted Impregnation. *Appl. Catal., B* **2021**, *296*, 120322.
(56) Karouia, F.; Boualleg, M.; Digne, M.; Alphonse, P. Control of the Textural Properties of Nanocrystalline Boehmite (γ-AlOOH) Regarding Its Peptization Ability. *Powder Technol.* **2013**, *237*, 602−609.
(57) Debecker, D. P.; Kuok (Mimi) Hii, K.; Moores, A.; Rossi, L. M.; Sels, B.; Allen, D. T.; Subramaniam, B. Shaping Effective Practices for Incorporating Sustainability Assessment in Manuscripts Submitted to ACS Sustainable Chemistry & Engineering: Catalysis and Catalytic Processes. *ACS Sustain. Chem. Eng.* **2021**, *9* (14), 4936−4940.
(58) Kwak, J. H.; Kovarik, L.; Szanyi, J. CO2 Reduction on Supported Ru/Al2O3 Catalysts: Cluster Size Dependence of Product Selectivity. *ACS Catal.* **2013**, *3* (11), 2449−2455.
(59) Lafficher, R. Nouveau procédé de précipitation pour la synthèse d'alumine, Ph.D Thesis, Université de Lyon, 2016. https://tel.archives-ouvertes.fr/tel-01425446 (accessed 2022−07−22).
(60) Lafficher, R.; Digne, M.; Salvatori, F.; Boualleg, M.; Colson, D.; Puel, F. Ammonium Aluminium Carbonate Hydroxide NH4Al(OH)-2CO3 as an Alternative Route for Alumina Preparation: Comparison with the Classical Boehmite Precursor. *Powder Technol.* **2017**, *320*, 565−573.
(61) Massiot, D.; Fayon, F.; Capron, M.; King, I.; Le Calvé, S.; Alonso, B.; Durand, J.-O.; Bujoli, B.; Gan, Z.; Hoatson, G. Modelling One- and Two-Dimensional Solid-State NMR Spectra. *Magn. Reson. Chem.* **2002**, *40* (1), 70−76.
(62) Barrett, E.; Joyner, L.; Halenda, P. The Determination of Pore Volume and Area Distributions in Porous Substances. I. Computations from Nitrogen Isotherms. *J. Am. Chem. Soc.* **1951**, *73* (1), 373−380.